Ferromagnetic Weyl Semimetals

9TH CONFERENCE ON CHIRALITY, VORTICITY AND MAGNETIC FIELDS IN QUANTUM MATTER, Sao Paulo 8 July 2025

Dima Cheskis

Ariel University

July 8, 2025

Combined ferromagnetic and topological effect

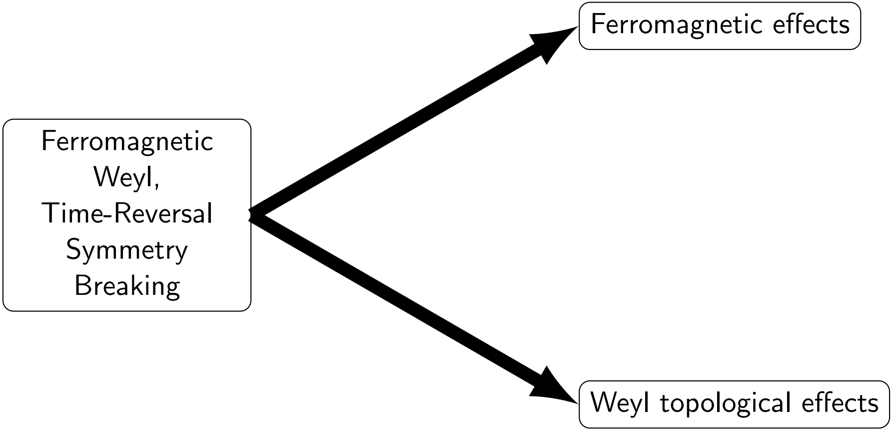

Semiclassical Dynamics and Bloch Functions

Bloch state:

$$\psi_{\mathbf{k}}(\mathbf{r}) = e^{i\mathbf{k}\cdot\mathbf{r}} u_{\mathbf{k}}(\mathbf{r})$$

Wave packet constructed from Bloch states:

$$\Psi(\mathbf{r}, t) = \int d\mathbf{k}\, a(\mathbf{k}, t)\, \psi_{\mathbf{k}}(\mathbf{r})$$

Where: $a(\mathbf{k}, t)$ is sharply peaked around $\mathbf{k}_c(t)$

Real-space form of the wave packet:

$$\Psi(\mathbf{r}, t) \approx e^{i\mathbf{k}_c\cdot(\mathbf{r}-\mathbf{r}_c)} f(\mathbf{r} - \mathbf{r}_c)$$

Smooth Evolution of Bloch States and Berry Connection

Instantaneous eigenstate of the time-independent Hamiltonian:

$$\hat{H}(\mathbf{k}(t))u_{\mathbf{k}(t)} = \varepsilon(\mathbf{k}(t))u_{\mathbf{k}(t)}$$

Time evolution of the Bloch state:

$$\frac{d}{dt}u_{\mathbf{k}(t)} = \dot{\mathbf{k}} \cdot \nabla_{\mathbf{k}} u_{\mathbf{k}}$$

Berry connection:

$$\boldsymbol{\mathcal{A}}(\mathbf{k}) = i\langle u_{\mathbf{k}} | \nabla_{\mathbf{k}} u_{\mathbf{k}} \rangle$$

Berry Phase Rate and Accumulation

Projecting onto the state itself gives the geometric phase rate:

$$i \left\langle u_{\mathbf{k}(t)} \middle| \frac{d}{dt} u_{\mathbf{k}(t)} \right\rangle = \dot{\mathbf{k}} \cdot \boldsymbol{\mathcal{A}}(\mathbf{k}(t))$$

Berry phase accumulated over time:

$$\gamma(t) = \int_0^t \dot{\mathbf{k}}(t') \cdot \boldsymbol{\mathcal{A}}(\mathbf{k}(t'))\, dt' = \int_{\mathbf{k}(0)}^{\mathbf{k}(t)} \boldsymbol{\mathcal{A}}(\mathbf{k}) \cdot d\mathbf{k}$$

Semiclassical Dynamics: Lagrangian + Final Equation of Motion

Lagrangian:

$$\mathcal{L} = (\mathbf{k} + e\mathbf{A}(\mathbf{r})) \cdot \dot{\mathbf{r}} - \varepsilon(\mathbf{k}) + e\phi(\mathbf{r}) + \dot{\mathbf{k}} \cdot \boldsymbol{\mathcal{A}}(\mathbf{k})$$

Step 1: Euler–Lagrange for r

$$\frac{\partial \mathcal{L}}{\partial \dot{\mathbf{r}}} = \mathbf{k} + e\mathbf{A}(\mathbf{r})$$

$$\Rightarrow \dot{\mathbf{k}} = -e\left(\mathbf{E} + \dot{\mathbf{r}} \times \mathbf{B}\right)$$

Step 2: Euler–Lagrange for k

$$\frac{\partial \mathcal{L}}{\partial \dot{\mathbf{k}}} = \boldsymbol{\mathcal{A}}(\mathbf{k})$$

$$\Rightarrow \dot{\mathbf{r}} = \nabla_{\mathbf{k}}\varepsilon(\mathbf{k}) - \dot{\mathbf{k}} \times \boldsymbol{\Omega}(\mathbf{k})$$

Final Equations of Motion:

$$\boxed{\begin{aligned} \dot{\mathbf{k}} &= -e\left(\mathbf{E} + \dot{\mathbf{r}} \times \mathbf{B}\right) \\ \dot{\mathbf{r}} &= \nabla_{\mathbf{k}}\varepsilon(\mathbf{k}) - \dot{\mathbf{k}} \times \boldsymbol{\Omega}(\mathbf{k}) \end{aligned}}$$

Crystal and Magnetic Structure of $Co_3Sn_2S_2$

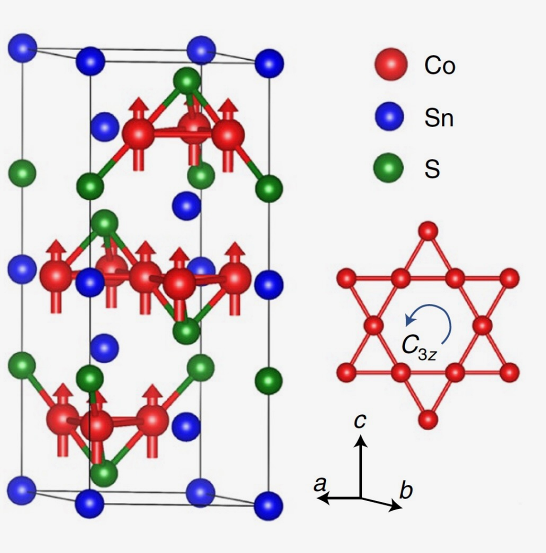

Energy Dispersion of $Co_3Sn_2S_2$

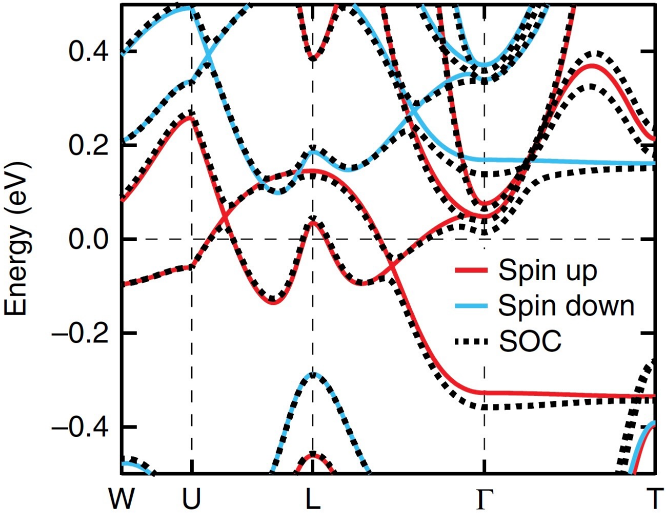

Weyl Hamiltonian and Eigenstates

Consider a Weyl node at momentum $\mathbf{k}_W$. Define the displacement from the node:

$$\mathbf{q} = \mathbf{k} - \mathbf{k}_W$$

The low-energy Weyl Hamiltonian is:

$$\boxed{H(\mathbf{q}) = \chi\, \boldsymbol{\sigma} \cdot \mathbf{q}}$$

Its eigenvalues are:

$$\boxed{\varepsilon_\pm(\mathbf{q}) = \pm|\mathbf{q}|}$$

In spherical coordinates, the positive-energy eigenstate (conduction band) is:

$$|u_+(\mathbf{q})\rangle = \begin{pmatrix} \cos\frac{\theta}{2} \\ \sin\frac{\theta}{2} e^{i\phi} \end{pmatrix}$$

Berry Curvature of Weyl point

The Berry curvature is derived from the Berry connection:

$$\boxed{\boldsymbol{\Omega}(\mathbf{q}) = \nabla_{\mathbf{q}} \times \mathbf{A}(\mathbf{q}) = \frac{1}{2}\frac{\mathbf{q}}{|\mathbf{q}|^3}}$$

- This expression represents the field of a monopole located at the Weyl point $\mathbf{k}_W$.
- The Weyl node acts as a source or sink of Berry flux, depending on its chirality χ.

Phase-Space Modification, Chiral Anomaly, and CME

Phase-Space Modification

Berry curvature modifies the phase-space density of states:

$$D(\mathbf{k}) = 1 + \frac{e}{\hbar}\mathbf{B} \cdot \mathbf{\Omega}(\mathbf{k})$$

Chiral Anomaly in k-Space

From the semiclassical Boltzmann equation with Berry curvature corrections:

$$\frac{d\rho_5}{dt} = \frac{e^3}{4\pi^2\hbar^2}\mathbf{E} \cdot \mathbf{B}$$

where ρ_5 is the chiral charge density.

Chiral Magnetic Effect (CME):

$$\mathbf{J}_{\mathrm{CME}} = \frac{e^2}{4\pi^2\hbar^2 c}\mu_5\,\mathbf{B}$$

where μ_5 is the chiral chemical potential.

[D. E. Kharzeev, Chiral Magnetic Effect]

Negative Magnetoresistance and Chiral Imbalance Relaxation

$$\mathbf{J}_{\mathrm{CME}} \propto \mu_5 \mathbf{B} \quad \Rightarrow \quad \textbf{Negative Magnetoresistance (NMR)}$$

Relaxation Dynamics

Chiral imbalance relaxes via inter-valley scattering, characterized by a relaxation time τ_v:

$$\frac{d\rho_5}{dt} = \frac{e^3}{4\pi^2\hbar^2}\,\mathbf{E}\cdot\mathbf{B} - \frac{\rho_5}{\tau_v}$$

Conclusion

NMR occurs when $\mathbf{E} \parallel \mathbf{B}$, and its magnitude is influenced by the chiral node separation, different types of disorder, and electron-phonon scattering.

NMR Properties

- Negative magnetoresistance (NMR) appears only when $\mathbf{E} \parallel \mathbf{B}$; for $\mathbf{E} \perp \mathbf{B}$, a positive magnetoresistance is typically observed.
- NMR is strongest when $\mathbf{E} \parallel \mathbf{B} \parallel \mathbf{b}$, where $\mathbf{b}$ is the chiral separation vector between Weyl nodes.
- The chiral vector $\mathbf{b}$ is aligned with the easy axis of magnetization: $\mathbf{b} \parallel \mathbf{M}_{\text{easy}}$.
- The chiral magnetic current follows:

$$\mathbf{J}_{\text{CME}} \propto \mu_5 \mathbf{B} \propto (\mathbf{E} \cdot \mathbf{B})\, \mathbf{B} \Rightarrow \sigma(B) - \sigma(0) \propto B^2, \quad \text{for small } \mu_5.$$

NMR, Previous Experiments

- For $\vec{B} \perp \vec{I}$ ($\theta = 90°$), a positive magnetoresistance is observed.
- For $\vec{B} \parallel \vec{I}$ ($\theta = 0°$), a negative magnetoresistance is demonstrated.
- The magnetoconductance for $\vec{B} \parallel \vec{I}$ follows a near-parabolic dependence: $\sigma(B) - \sigma(0) \propto B^{1.9}$ up to 14 T.

E. Liu *et al.*, *Giant anomalous Hall effect in a ferromagnetic kagome-lattice semimetal*, Nature Physics **14**, 1125–1131 (2018), https://doi.org/10.1038/s41567-018-0234-5

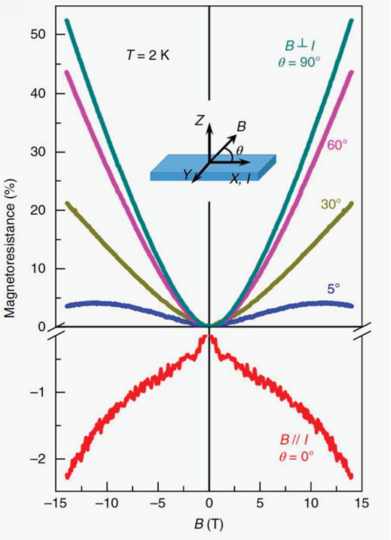

Sample scheme with electronic contacts

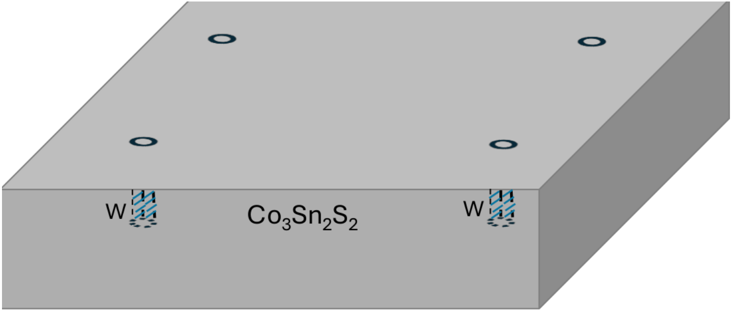

Figure 1: Description of the first image

Sample scheme with electronic contacts

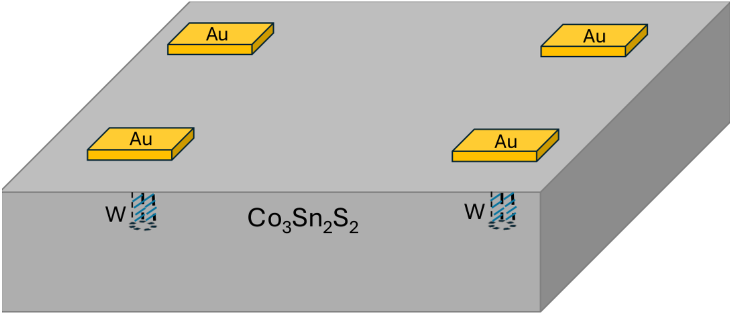

Figure 2: Description of the second image

Sample scheme with electronic contacts

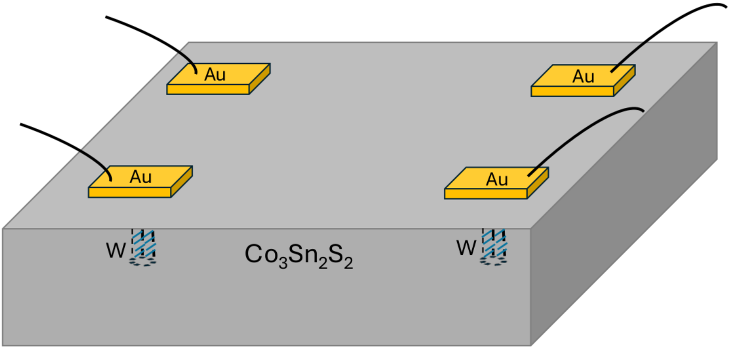

Figure 3: Description of the third image

Sample scheme with electronic contacts

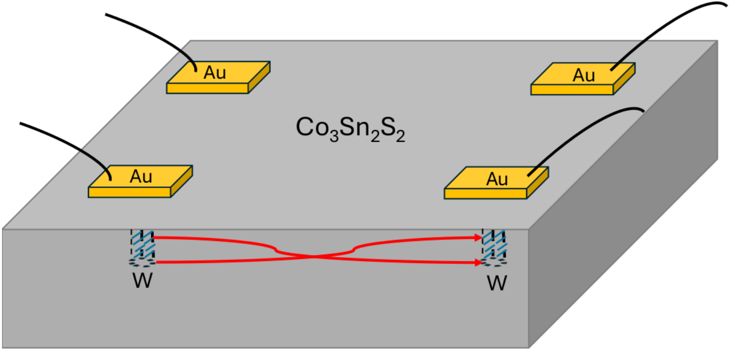

Figure 4: Description of the fourth image

Magnetoresistance at 0°

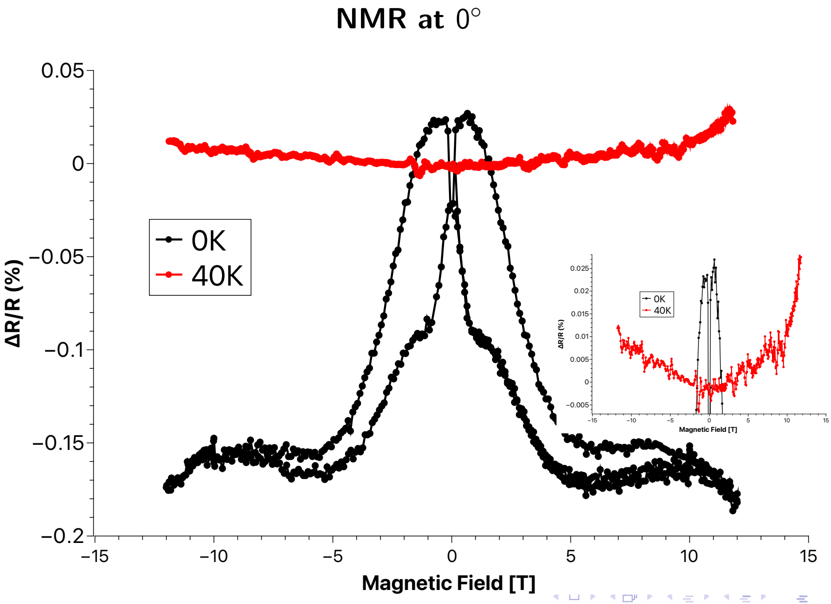

Zoomed View: Magnetoresistance at 0°

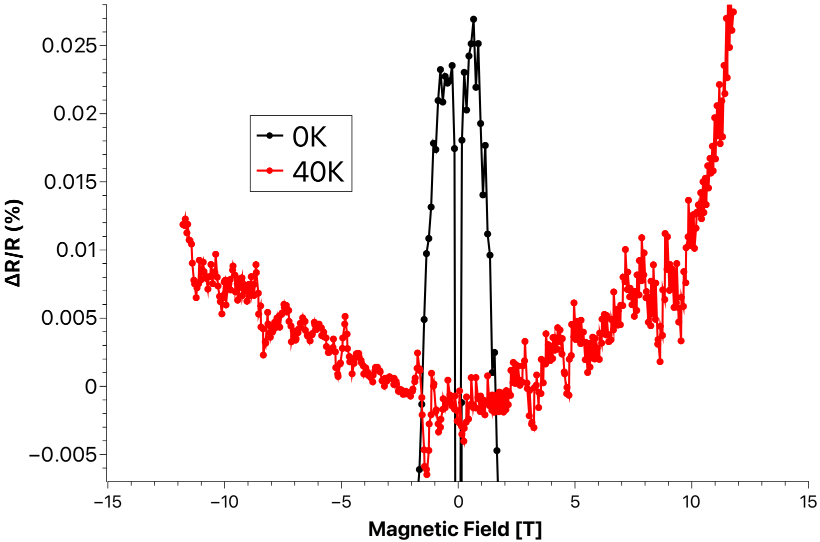

Magnetoresistance at 90°

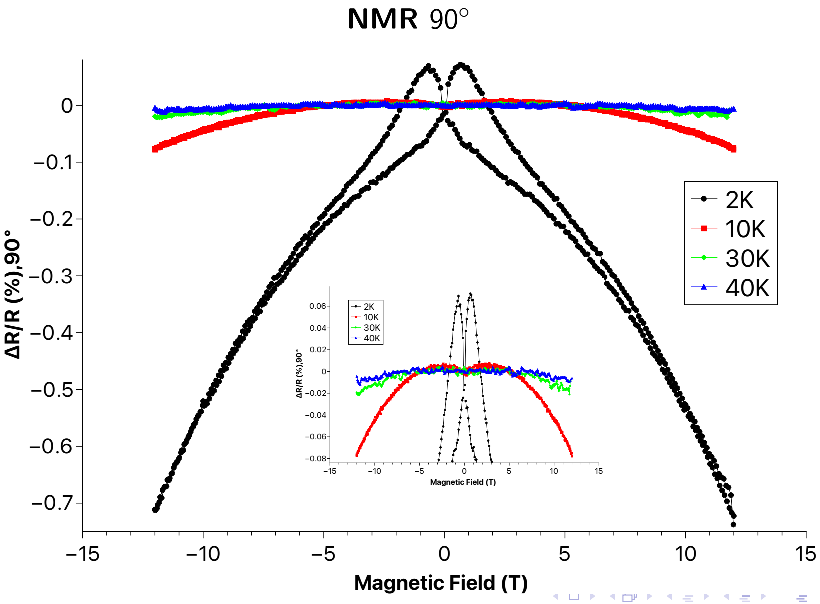

Zoomed View: Magnetoresistance at 90°

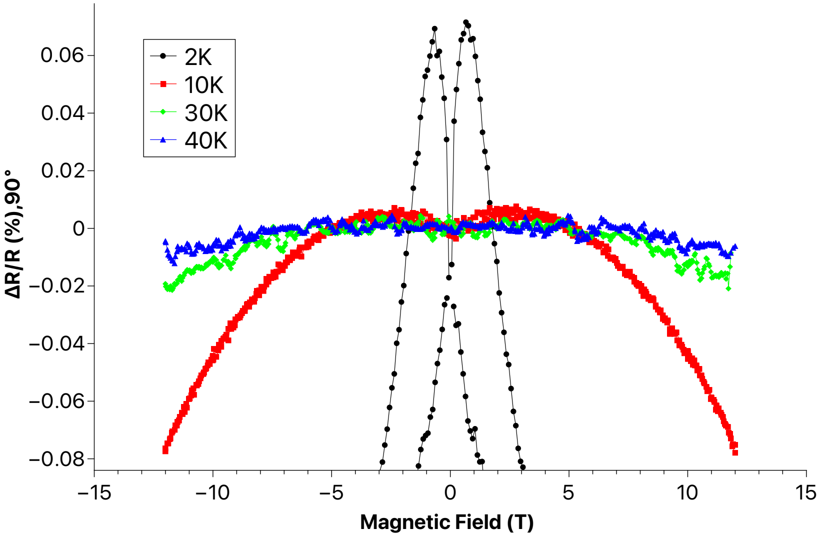

Relative Magnetoconductivity

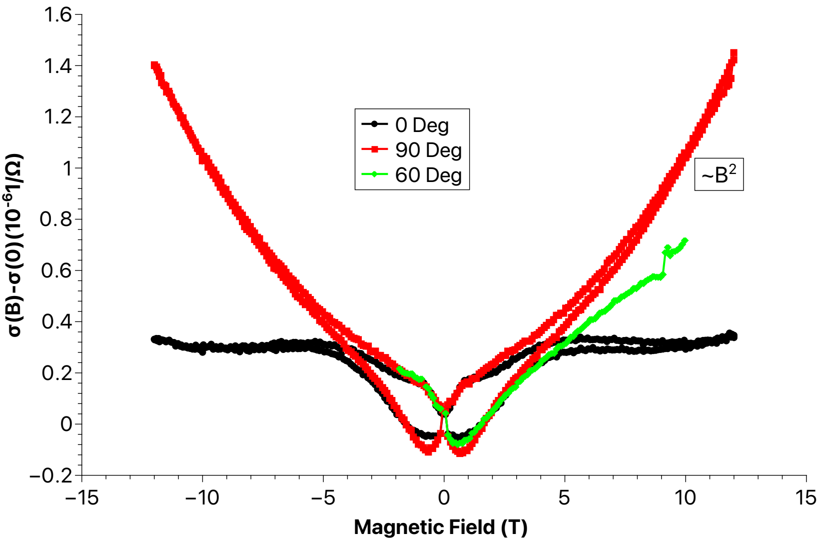

Conclusions and Future Plans

Conclusions

- **Negative Magnetoresistance (NMR):** Strongly observed when the magnetic field is applied parallel to the c-axis, and remains negative up to 40 K. Maximum effect occurs for $\mathbf{E} \parallel \mathbf{B} \parallel \mathbf{b}$.
- **Hysteresis in Magnetoresistance:** Angular dependence of NMR appears only above 5 Tesla.
- **Magnetoconductance Behavior:** Displays B^2 dependence only when NMR is aligned with the c-axis and field exceeds 5 Tesla.

Future Plans

- **Complete DC NMR Measurements:** Finalize the set of DC magnetoresistance experiments.
- **AC NMR:** Perform AC magnetoresistance measurements to probe intervalley scattering time.
- **ARPES:** Conduct angle-resolved photoemission spectroscopy to map the electronic band structure.